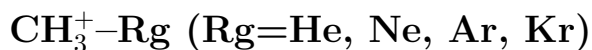


Vibrational analysis of methyl cation – rare gas atom complexes:



Jan Meisner, Philipp P. Hallmen, Johannes Kästner and Guntram Rauhut*

Institute for Theoretical Chemistry, University of Stuttgart,

Pfaffenwaldring 55, D-70569 Stuttgart, Germany

Abstract

The vibrational spectra of simple $\text{CH}_3^+ - \text{Rg}$ (Rg=He, Ne, Ar, Kr) complexes have been studied by vibrational configuration interaction (VCI) theory relying on multidimensional potential energy surfaces (PES) obtained from explicitly correlated coupled cluster calculations, CCSD(T)-F12a. In agreement with experimental results, the series of rare gas atoms leads to rather unsystematic results and indicates huge zero point vibrational energy effects for the helium complex. In order to study these sensitive complexes more consistently, we also introduce configuration averaged vibrational self-consistent field theory (CAVSCF), which is a generalization of standard VSCF theory to several configurations. The vibrational spectra of the complexes are compared to that of the methyl cation, for which corrections due to scalar-relativistic effects, high-level coupled-cluster terms, i.e. CCSDTQ, and core-valence correlation have explicitly been accounted for. The occurrence of tunneling splittings for the vibrational ground-state of $\text{CH}_3^+ - \text{He}$ has been investigated on the basis of semiclassical instanton theory. These calculations and a direct comparison of the energy profiles along the intrinsic reaction coordinates (IRC) with that of the hydronium cation, H_3O^+ , suggest that tunneling effects for vibrationally excited states should be very small.

* To whom correspondence should be addressed: rauhut@theochem.uni-stuttgart.de

I. INTRODUCTION

The spectroscopic investigation of ionic complexes is a challenging task and is usually accompanied by *ab initio* calculations to guide the interpretation of the observed spectra.¹⁻⁷ However, as these clusters are often very floppy, they request a proper account of anharmonic corrections and correlation effects in order to yield reliable results. Complexes of the methyl cation with rare gas atoms have extensively been studied by Dopfer and co-workers and a wealth of information is available for these systems.¹⁻⁵ These authors used infrared photodissociation spectroscopy in combination with *ab initio* calculations at the MP2 level with a modified aug-cc-pVTZ basis set to gain an understanding of the structural and vibrational properties of these complexes. Of course, 2nd order Møller-Plesset perturbation theory is limited in accuracy and predictions are often of qualitative rather than quantitative nature. Moreover, the harmonic approximation leaves many questions open and thus an anharmonic treatment of these systems is highly desirable. Consequently, Dopfer and co-workers concluded that *future efforts to explore the properties of the intermolecular interaction in CH_3^+-He in a more quantitative way will require a potential energy surface that takes monomer relaxation into account.* This prompted Asvany and collaborators to perform calculations employing 2nd order vibrational perturbation theory, VPT2,⁸ to account for anharmonicity effects in the CH_3^+-He complex. These authors used more reliable coupled cluster calculations, i.e. CCSD(T)/cc-pVTZ, to determine a quartic force field of the potential energy surface.⁶ The same way, all calculations presented here use high-level explicitly correlated coupled-cluster theory to determine a multi-dimensional potential energy surface without imposing any constraints on the coordinates.

It was found, that the structures of CH_3^+-Rg clusters are strongly dependent on the size of the rare gas atom. For example, while complexation with helium leads to a very moderate distortion of the CH_3^+ moiety, the interaction with an argon or krypton atom results in a pronounced pyramidalization of the methyl cation. For a detailed discussion of that issue see Ref. 5 and references therein. Besides that, the zero point vibrational energy leads to large corrections in the He cluster, while the effects are less dramatical for Ar or Kr complexes. A proper quantization of these effects requests high-level electronic structure calculations in combination with high-dimensional variational calculations for determining

vibrational wavefunctions.

A particular aspect concerns tunneling splitting within these complexes.¹⁻⁵ As the dominant interaction within these complexes is associated with the $2p_z$ orbital of the planar (D_{3h}) methyl cation, the rare gas atom can be bound to either side of it. This results in two equivalent minima, which are mainly connected by a movement of the hydrogen atoms - rather than a large amplitude motion of the rare gas atom around the CH_3^+ moiety. The formal transition state associated with the minimum energy path is planar and shows C_{2v} symmetry. Consequently, tunneling splitting may formally occur in all of these complexes. Based on calculations on a 3-dimensional energy surface of the interaction potential at the MP2 level (keeping all intramolecular coordinates of the CH_3^+ moiety frozen), significant splittings were found for the bending and stretching modes in the CH_3^+-He complex and a splitting of about 0.008 cm^{-1} for the vibrational ground state.⁴ In contrast to that recent studies by Töpfer *et al.* based on double resonance rotational spectroscopy do not confirm this result.⁹ Therefore, we will consider this aspect in some detail.

Within the course of this study, we introduce and use configuration-averaged vibrational self-consistent field theory (CAVSCF) to determine optimized one-mode wavefunctions in order to avoid symmetry-broken solutions in the subsequent vibrational configuration interaction calculations (VCI). This concept has been developed many years ago within electronic structure theory and has been revived within the context of calculating crystal field splittings for molecular magnets.¹⁰⁻¹² However, this theory has not yet been transferred to the solution of the vibrational Schrödinger equation. For that reason, we will outline the basics of this theory briefly.

II. CONFIGURATION AVERAGED VSCF THEORY

In order to keep the equations as simple as possible, we will neglect the vibrational angular momentum terms¹³ and the Watson correction term as occurring in the Eckart-Watson Hamiltonian.¹⁴ In all what follows the multidimensional potential energy surface shall be represented by an n -mode representation¹⁵ expressed in polynomials, i.e.

$$V(\mathbf{q}) = V_{1D} + V_{2D} + V_{3D} + \dots \quad (1)$$

with

$$V_{1D} = \sum_i \sum_r p_r^{(i)} q_i^r \quad (2)$$

$$V_{2D} = \sum_{i < j} \sum_{rs} p_{rs}^{(ij)} q_i^r q_j^s \quad (3)$$

$$V_{3D} = \dots \quad (4)$$

q_i^r denotes a polynomial of order r for mode i , while p are the associated coefficients as obtained from fitting procedures.¹⁶ Note, by definition $p_{rs}^{(ii)} = 0$, $p_{rst}^{(ij)} = 0$ etc. Within VSCF theory the wave function is given as a product of modals φ_i^I belonging to configuration I :

$$\Psi^I = \prod_i \varphi_i^I(q_i) \quad \text{with} \quad \varphi_i^I = \sum_\mu C_{\mu i}^I \chi_{\mu i} \quad (5)$$

$\chi_{\mu i}$ are the basis functions, e.g. harmonic oscillator function or distributed Gaussians, and $C_{\mu i}^I$ are the modal coefficients to be optimized within the VSCF iterations. We will employ the integrals

$$Q_{\mu\nu}^{ir} = \langle \chi_{\mu i} | q_i^r | \chi_{\nu i} \rangle \quad \text{and} \quad X_{ir}^I = \sum_{\mu\nu} C_{\mu i}^I C_{\nu i}^I Q_{\mu\nu}^{ir} \quad (6)$$

A. Standard VSCF Theory

Using the n -mode representation of the potential and the aforementioned definitions, the energy expectation value within VSCF theory^{17–19} can be written as

$$E_I = \sum_i \sum_{\mu\nu} C_{\mu i}^I C_{\nu i}^I \left[-\frac{1}{2} T_{\mu\nu}^i + \sum_r Q_{\mu\nu}^{ir} [p_r^{(i)} + \sum_j \sum_s X_{js}^I \left[\frac{1}{2} p_{rs}^{(ij)} + \dots \right]] \right] \quad (7)$$

Herein $T_{\mu\nu}^i$ denotes the kinetic energy associated with mode i in the basis of the primitive functions. As these functions are mode-dependent, the integral of the kinetic energy also depends on the mode. Requesting normality of all modals for each mode yields the Lagrangian

$$L = E_I - \sum_i \varepsilon_i^I (\langle \varphi_i^I | \varphi_i^I \rangle - 1) \quad (8)$$

Variation of the Lagrangian with respect to the modal coefficients finally leads to a generalized eigenvalue equation with the hermitian Fock-type matrix

$$F_{\mu\nu}^{i,I} = -\frac{1}{2} T_{\mu\nu}^i + \sum_r Q_{\mu\nu}^{ir} \bar{p}_r^{(i),I} \quad (9)$$

where $\bar{p}_r^{(i),I}$ denotes the effective potential given as

$$\bar{p}_r^{(i),I} = p_r^{(i)} + \sum_j \sum_s X_{js}^I \left[p_{rs}^{(ij)} + \sum_k \sum_t \left[\frac{1}{2} p_{rst}^{(ijk)} + \dots \right] \right] \quad (10)$$

As the Fock-type matrix \mathbf{F} depends on the modal coefficients, the equations must be solved iteratively until self-consistency is achieved, which is responsible for the name of this procedure.

B. CAVSCF Theory

In order to optimize the modals for degenerate states in molecules belong to non-Abelian point groups, VSCF theory can be generalized to several configurations by simple averaging. Assuming identical weights for all configurations to be considered in CAVSCF, the energy expression is given as

$$E_{\text{CA}} = \frac{1}{N} \sum_I E_I \quad (11)$$

where N is the number of configurations to be considered. We further introduce a fractional occupation number γ_{a_i} for modal a_i of mode i

$$\gamma_{a_i} = \frac{n_{a_i}}{N} \quad (12)$$

where n_{a_i} is the number of configurations, in which the modal a_i of mode i is used. The condition

$$\sum_{a_i} \gamma_{a_i} = 1 \quad (13)$$

must hold for every mode i . Clearly, the weight factors γ simply depend on the configurations to be considered simultaneously. With this, eq. 7 can be generalized to

$$E_{\text{CA}} = \sum_i \sum_{a_i} \gamma_{a_i} \sum_{\mu\nu} C_{\mu i}^{a_i} C_{\nu i}^{a_i} \left[-\frac{1}{2} T_{\mu\nu}^i + \sum_r Q_{\mu\nu}^{ir} [p_r^{(i)} + \sum_j \sum_{b_j} \gamma_{b_j} \sum_s X_{js}^{b_j} \left[\frac{1}{2} p_{rs}^{(ij)} + \dots \right]] \right] \quad (14)$$

Likewise, the Lagrangian can now be written by extending it to all active modals within each mode i :

$$L_{\text{CA}} = E_{\text{CA}} - \sum_i \sum_{a_i b_i} \varepsilon_i^{a_i b_i} (\langle \varphi_i^{a_i} | \varphi_i^{b_i} \rangle - \delta_{a_i b_i}^i) \quad (15)$$

Variation of the Lagrangian finally yields a Fock-type matrix given as

$$F_{\mu\nu}^{i,\text{CA}} = -\frac{1}{2}T_{\mu\nu}^i + \sum_r Q_{\mu\nu}^{ir} \left[p_r^{(i)} + \sum_j \sum_{b_j} \gamma_{b_j} \sum_s X_{js}^{b_j} \left[\frac{1}{2}p_{rs}^{(ij)} + \dots \right] \right] \quad (16)$$

Comparison of the equations for CAVSCF and VSCF theory reveals, that besides the introduction of fractional occupations γ_{a_i} it is simply an additional loop over the active modals and the extension of the contracted integrals \mathbf{X} to all active modals rather than just one modal in standard VSCF theory. However, this does not lead to any storage problems. Consequently, CAVSCF theory is a rather simple generalization of VSCF theory, which is just the special case for one configuration. Using identical weights for the individual configurations of degenerate states, CAVSCF can be used for determining state-specific solutions without symmetry breaking within the calculation of degenerate states in non-Abelian molecules.

III. INSTANTON THEORY

To quantify the tunneling splitting of the CH_3^+ -He cluster in the vibrational ground state, we used semiclassical instanton theory.^{20–23} In instanton theory, the tunneling splitting Δ is calculated by the ratio of the partition function of the full quantum system, $Q(\beta)$, and the partition function of the non-tunneling system, $Q_0(\beta)$

$$\lim_{\beta \rightarrow \infty} \frac{Q(\beta)}{Q_0(\beta)} = \cosh \left(\frac{\beta \Delta}{2} \right), \quad (17)$$

where $\beta = \frac{1}{k_B T}$ is the inverse temperature and k_B is Boltzmann's constant. To calculate the partition function of the full system, $Q(\beta)$, in principle all paths from one minimum to the other should be considered following Feynman's idea of path integrals. However, in instanton theory the most likely tunneling path, the so-called instanton, is optimized and the steepest-descent integration around it is used. Thus, quantum fluctuations about this path are considered in harmonic approximation by diagonalization of the Hessian matrix of the full instanton. Along the tunneling path, full anharmonicity is included, and, thus, instanton theory can be considered to be correct by an order of magnitude.²⁴

IV. COMPUTATIONAL DETAILS

Explicitly correlated coupled-cluster calculations, CCSD(T)-F12a and CCSD(T)-F12b,²⁵ in combination with an augmented triple- ζ basis, i.e. aug-cc-pVTZ,²⁶ have been used to determine the structures of all complexes and the bare methyl cation, as well as for the instanton calculations. Note that we used F12a theory for the calculation of all clusters, but employed F12b calculations for the monomer for which we also used larger basis sets. In general F12b theory shows slightly better performance for large basis sets than the F12a approximation. These levels can roughly be compared with conventional coupled-cluster calculations relying on an augmented quintuple- ζ basis set.²⁷ At the same level of theory, harmonic frequencies and normal coordinates as needed for spanning the potential energy surface have been determined. For all calculations we used the MOLPRO package of *ab initio* programs.²⁸

We used n -mode representations¹⁵ of the potential energy surfaces truncated after the 4-mode coupling terms within the vibrational configuration interaction calculations.^{29,30} Within all these calculations the expansion points of the n -mode representations were chosen to be the equilibrium structures, i.e. local PESs were generated, which harbor just one of the two possible minima. A multi-level scheme has been exploited, in which the 1-mode and 2-mode coupling terms were determined at the CCSD(T)-F12a/aug-cc-pVTZ level, while the 3-mode and 4-mode coupling terms were obtained from CCSD(T)-F12a/aug-cc-pVDZ theory. In order to exploit symmetry within the PES generation more efficiently, the displacement vectors of the degenerate normal coordinates were rotated by $\pi/4$ as described most recently.³¹ The resulting grid representation of the potential was transformed into an analytical representation based on polynomials up to 7th order. For the transformation we used our recently developed algorithm relying on Kronecker products.¹⁶ Initial vibrational wavefunctions were obtained from vibrational self-consistent field theory employing a mode-specific basis of 20 distributed Gaussians. For this, the Watson Hamiltonian¹⁴ has been used, in which the μ -tensor was truncated after the 0th order term.¹³ The subsequent VCI calculations were based on Hartree products (configurations) generated from the VSCF modals (one-mode wavefunctions) of the vibrational ground-state. The correlation space within the VCI calculations was limited to 6-tuple excitations up to

the 7th root and a maximum sum of quantum numbers of 25. A configuration-selective VCI approach^{29,30} based on VSCF modals of the vibrational ground-state or modals obtained from CAVSCF theory have been used to limit the computational effort in this step. Symmetry breakings due to insufficiencies in the potential, fitting to the polynomials or limitations of the configuration space etc. were found to be as small as 0.01 cm^{-1} .

Instantons were calculated at 2.0 K and 1.75 K using a quasi-Newton-Raphson algorithm.³² Note that for the tunneling splitting, the limit of zero temperature is required, cf. Eq. 17. Here, the temperature is a parameter rather than a physical quantity. 610 images were used for the discretization of the instanton path. Instanton paths were considered to be converged when the maximum component of the gradient (in atomic units, i.e. $m_e = 1$) was below 10^{-8} . The rotational contribution to the partition function of the instanton and the minimum structure was approximated as classical rigid rotors. For the calculation of the intrinsic reaction coordinate (IRC) and the the instanton calculations the DL-Find optimization library was used.³³ The communication between DL-Find and MOLPRO²⁸ was realized using the Chemshell interface.³⁴ For the IRC optimization, the Hessian predictor-corrector algorithm^{35,36} has been applied as recently implemented in DL-Find.³⁷ A step size of 0.02 a.u. was used to optimize the IRC on the comparably flat PES. To obtain a smooth gradient, we tightened the SCF and CCSD(T) convergence to 10^{-11} Hartree for the calculation of the IRC, instantons, and Hessians along the instanton pathways.

V. RESULTS AND DISCUSSION

A. Geometrical parameters

While the equilibrium structure of a molecule is uniquely defined, there are several possibilities concerning vibrationally averaged structures. Usually, the definitions differ with respect to the operator within the integral of the expectation value. We employed internal coordinates, i.e. bond lengths etc., which were expanded in terms of normal coordinates, the latter also being used as variables for the wavefunctions. Temperature effects by Boltzmann weighting were not included in these calculations. Structural parameters being most important for this study here are listed in Table I. According to Table I and as discussed in detail

by Dopfer and co-workers³ the interaction of the Ar and Kr atoms with the methyl cation are much stronger than for the other two systems, which leads to a pronounced pyramidalization of the CH_3^+ moiety in contrast to the helium or neon complexes. However, this effect appears to be less pronounced by the coupled-cluster calculations presented here in comparison to the MP2 results of the literature.^{1-3,5} Our CCSD(T)-F12a results also indicate a weaker pyramidalization due to neon than to helium, which is not supported by the MP2 results. However, the effects are rather weak and surely within the error bar of the MP2 calculations. Nevertheless, this result is counter-intuitive as neon shows a larger polarizability than helium and thus one would expect a stronger pyramidalization. The calculated interaction energy of the neon-complex is also computed to be larger than for helium (see below). However, due to the bigger covalent radius, the C–Ne distance is significantly longer than the C–He distance in the helium complex and thus there appears to be a sensitive equilibrium between the contributing physical forces. The differences between the vibrationally averaged C–Rg distances, $R_0(\text{C-Rg})$, and the corresponding values within the equilibrium structures, i.e. $\Delta R_{\text{e}0}(\text{C-Rg})$, are in nice agreement with the estimates of Dopfer and co-workers (cf. the comparison in Table I).^{1,2} Note that these values cannot directly be compared as Dopfer and co-workers determined the difference in a pseudo-diatomic system and thus these authors refer to the center of mass of the CH_3^+ moiety, while our values refer to the true atom-atom distances. As the pyramidalization is largest for the Ar and Kr clusters, the largest difference between our $\Delta R_{\text{e}0}(\text{C-Rg})$ values and the related results of Dopfer and co-workers must arise for these particular systems. Table I clearly supports the known result, that huge ZPVE effects can be found for the CH_3^+ –He complex. The unsystematic behavior of the C–Rg distances is visualized in Figure 1. As must be expected, the ZPVE effects are less pronounced in the deuterated CD_3^+ –Rg complexes. The corresponding values are listed in Table II.

B. Energetic considerations

Complexation energies, E_{Cplx} , relaxation energies, E_{Relax} , and dissociation energies, $D_e = E_{\text{Cplx}} - E_{\text{Relax}}$, of the CH_3^+ –Rg complexes are shown in Table III. Clearly, the complexation energies and the dissociation energies grow with increasing period of the rare gas atoms. However, this does not hold true for the relaxation energy of the CH_3^+

moiety, which is in agreement with the pyramidalization as discussed above, i.e. for the neon complex the pyramidalization (see $\Delta R_e(\text{C-H}_3)$ in Table I) is less pronounced than for helium and likewise is the relaxation energy. Moreover, as discussed in detail by Dopfer and co-workers, the ZPVE has a huge effect on the dissociation energy of CH_3^+-He , which steadily decreases with the period of the rare gas atoms. All energies listed in Table III are much larger for Ar and Kr than for He and Ne. This is in line with the conclusion of Dopfer and co-workers that *only the CH_3^+-Rg dimers with large rare gas ligands have bonds with substantial covalent character*. This result is also supported by natural population and bond analyses (NBO),³⁸ which show a covalent C-Rg bond for $\text{Rg}=\{\text{Ar}, \text{Kr}\}$ associated with a substantial charge transfer. For the small rare gas atoms, i.e. He and Ne, the NBO and the charge transfer cannot be seen. An analysis based on symmetry adapted perturbation theory (SAPT)³⁹ reveals, that in the latter two systems, the interaction energy is dominated by induction and to a lesser extent by dispersion. Again, this agrees with the conclusions of Dopfer.⁵ For the deuterated species, the D_0 values are 348.8 (He), 785.2 (Ne), 5717.3 (Ar) and 8781.4 cm^{-1} (Kr).

As mentioned above, the complexes discussed here allow for an internal rotation of the CH_3^+ moiety, which give rise to formal planar transition states of C_{2v} symmetry. We have computed these barriers to be 698.5 (He), 916.4 (Ne), 5891.7 (Ar) and 8763.8 cm^{-1} (Kr). Dopfer and co-workers reported these values to be about 600, 750, and 6000 cm^{-1} (He, Ne, Ar).² Clearly, the barriers for CH_3^+-Ar and CH_3^+-Kr are too high to show any impact on the vibrational structure. It is the covalent bond character, which hinders the internal rotation in the latter two complexes. However, for the helium and neon complexes, the barriers are just slightly below the dissociation channels (D_e) and are low enough that tunneling effects may lead to vibrational splittings as discussed by Dopfer and Luckhaus.⁴ We will discuss this aspect in detail below.

C. Vibrational frequencies

1. Methyl cation

The experimental determination of the fundamental modes of the bare methyl cation (D_{3h}) is a non-trivial task and several attempts have been undertaken to assign the individual modes.^{40–44} The only accurately determined frequency of the methyl cation is the degenerate CH stretching mode, which has been determined by Crofton *et al.*⁴⁰ using infrared spectroscopy to be 3108.4 cm^{-1} . The only other mode, which has been determined experimentally, is the out-of-plane umbrella mode ν_2 . From photoelectron spectroscopy this vibration was found at 1406 ± 30 , 1366 ± 20 and 1356 cm^{-1} , respectively, while ion pair imaging spectroscopy yielded a value of $1359\pm7\text{ cm}^{-1}$.^{41–44} A more recent measurement by Cunha de Miranda *et al.*⁴⁵ based on threshold photoelectron spectroscopy determined this fundamental at $1387\pm15\text{ cm}^{-1}$. The scattering of these values and the large error bars indicate the problems associated with the assignment of this particular band. For CD_3^+ the situation differs completely. Asvany *et al.*⁶ determined all fundamentals except the symmetric CD stretching mode, which are in nice agreement with our theoretical predictions (see below).

Due to its limited size, the methyl cation has theoretically been studied by many authors.^{45–48} Yu and Sears computed the anharmonic vibrational frequencies of the methyl cation and its deuterated isotopologue using CCSD(T) calculations at the basis set limit.⁴⁶ These authors applied a coordinate scaling procedure in order to compensate for systematic overestimations in their calculations, which was criticized in the work of Cunha de Miranda *et al.*⁴⁵ Moreover, Yu and Sears used a rather limited force field in contrast to the calculations of Keceli *et al.*,⁴⁷ Cunha de Miranda *et al.*⁴⁵ and our own calculations, which include some 11248 potential terms. The results of Keceli *et al.*⁴⁷ do not include corrections due to the vibrational angular momentum (VAM) terms, which were found to be very important by Cunha de Miranda *et al.*,⁴⁵ who determined corrections by up to 22 cm^{-1} . Therefore, we consider the most reliable values to be those of Cunha de Miranda *et al.*,⁴⁵ which essentially coincide with our own calculation. However, this must be expected as the setup of our calculations essentially is the same as theirs although we use an n -mode expansion truncated

after the 4-mode coupling terms rather than the 3-mode couplings. However, this simply indicates that the n -mode expansion of the potential energy surface is converged after the inclusion of the 3-mode coupling terms. Our results are summarized in Table IV.

In order to investigate the effect of core-valence correlation etc. on this small molecule, which has not yet been done in any of the preceding theoretical studies, we have performed additional calculations, which account for these contributions. In order to limit the computational effort within the generation of the potential energy surfaces, we used a multi-level scheme, i.e. these further corrections were applied to the 1D and 2D-terms of the n -mode expansion of the potential, while the 3D and 4D-terms were determined at the CCSD(T)-F12b/cc-pVTZ-f12 level only. Core-valence corrections were determined from conventional CCSD(T)/cc-pCVQZ calculation relative to frozen core CCSD(T)/cc-pVQZ results. This correction was found to be largest for the two CH-stretching modes ν_1 and ν_3 and accounted for 4.8 and 4.9 cm^{-1} , respectively. For the other two modes the correction was less than 2.0 cm^{-1} . Relativistic effects were determined from scalar-relativistic calculations employing a 2nd order Douglas–Kroll–Hess Hamiltonian.^{49,50} In these calculations a aug-cc-pwCVQZ-dk basis set has been used. These corrections were determined to be very small, they amounted to less than 0.6 cm^{-1} for all frequencies. In a last step we incorporated high-order coupled-cluster terms by using the GECCO suite of *ab initio* programs.^{51,52} As these calculations are very demanding, we used a standard cc-pVTZ basis set for CCSDT calculations and a cc-pVDZ basis within the CCSDTQ calculations. The calculations led to a lowering of the frequencies by up to -2.2 cm^{-1} . Besides these corrections to the potential energy surface, we also included linear terms in the expansion of the μ -tensor rather than the constant term only within the evaluation of the VAM corrections.¹³ However, these correction were found to be very small and accounted to not more than 0.4 cm^{-1} . Adding all these corrections yields our most reliable values for CH_3^+ , which are shown in the 3rd column of Table IV. Apparently, the inclusion of core-valence correlation provides the largest correction, which is partly compensated for by the high-level coupled-cluster terms. This effect is well-known and has been observed by several authors.^{53–55} The comparison of these results with our standard calculations at the CCSD(T)-F12b/cc-pVTZ-f12 level shows that the differences are fairly small, but relies on the error compensation of the aforementioned corrections.

For the deuterated isotopologue our VCI calculations are in excellent agreement with the

experimental results of Asvany *et al.*⁶ and the theoretical predictions of Cunha de Miranda *et al.*⁴⁵

2. $\text{CH}_3^+ - \text{Rg}$ complexes

Harmonic and anharmonic vibrational frequencies for all complexes are summarized in Tables V and VI. Concerning the $\text{CH}_3^+ - \text{He}$ frequencies, our results agree to within 10 cm^{-1} with the computational results of Asvany and collaborators⁶ – except for the intermolecular coupling modes. Note that Asvany *et al.* used 2nd order vibrational perturbation theory, VPT2, based on a quartic force field obtained from conventional CCSD(T)/aug-cc-pVTZ calculations. This readily explains the differences between their and our calculations. A comparison with the experimental data shows that the CH stretching modes are nicely reproduced by our calculations, while the bending modes of the CH_3^+ moiety show larger deviations. Although the interaction of the helium atom with the methyl cation is rather weak, its introduction leads to frequency shifts of more than 20 cm^{-1} (ν_2) with respect to the bare methyl cation.

Of particular interest are the intermolecular bending modes ν_b of $\text{CH}_3^+ - \text{He}$ and $\text{CD}_3^+ - \text{He}$. The most obvious and surprising effect concerning these modes are corrections due to anharmonicity of up to almost 50%. With increasing size of the rare gas atom, the strong anharmonicity of the intermolecular bending mode decreases and amounts to less than 3% in case of the $\text{CH}_3^+ - \text{Kr}$ complex (cf. Table V). The huge correction due to anharmonicity can already be seen in the VSCF calculations and prompted us to visualize the harmonic potential in comparison to the effective anharmonic potential within the VSCF calculation of the vibrational ground state of $\text{CH}_3^+ - \text{He}$, cf. Figure 2. Clearly, the effective potential shows a strong quartic contribution and thus the harmonic approximation must be considered a rather poor approximation for this particular mode.

While all intramolecular modes of the CH_3^+ and CD_3^+ moieties and the intermolecular stretching modes ν_s were found to be stable with respect to the correlation space within the VCI calculations, the degenerate bending modes are very sensitive concerning the correlation space and thus the nature of the underlying VSCF modals. In principle, the VCI

results should be independent of the nature of the one-mode wavefunctions employed in the configurations. However, this was not the case for the intermolecular bending mode. The VCI calculations for ν_b presented here, suffer from the fact, that the inclusion of high-lying correlation functions did not improve the results, but introduced instabilities arising from the low lying dissociation channel. Therefore, we had to limit the VCI space with respect to high excitations for the intermolecular stretching and the bending mode. As a results, the VCI calculations are not fully converged and do depend on the chosen basis. As must be expected, this problem vanishes for the clusters with larger values of D_0 and has not been observed for the clusters containing Ar and Kr. In order to minimize the observed instabilities we investigated different sets of modals. VCI calculations based on configurations built from a simple harmonic oscillator basis (without VSCF optimization) fail completely and yield results being significantly too high. On the other hand, standard state-specific VSCF modals lead to symmetry-broken solutions for these non-Abelian systems and are thus not a proper choice for these particular complexes. Therefore, we used modals obtained from ground-state VSCF calculations and from configuration averaged VSCF calculations (CAVSCF) comprising the two configurations of the degenerate bending modes. For the non-degenerate modes of course we did not use CAVSCF theory, but standard state-specific VSCF calculations. The resulting VCI frequencies for the intermolecular bending and stretching modes are summarized in Table VII. According to Table VII the stretching modes ν_s are not affected by this problem and the ground-state based VCI calculations (gs-VCI) essentially coincide with the state-specific VCI calculations (ss-VCI), which rely on CAVSCF modals for ν_b and standard state-specific VSCF modals for ν_s . Clearly, the instability is largest for CH_3^+-He and decreases with increasing values of D_0 . For CD_3^+-Ne the effect is in the range of the accuracy of our calculations and thus we consider this value to be trustworthy, while the other three values bear a large error bar. Note that, relying on VPT2 theory Asvany and co-workers⁶ determined ν_b of CH_3^+-He to be 237 cm^{-1} (cf. Table V), which indicates even larger anharmonicity corrections. However, it is well known that VPT2 theory yields excellent results for semi-rigid molecules, which are comparable to VCI results,⁵⁶ but it remains an open question if 2nd order perturbation theory can handle floppy systems, whose potential energy surface cannot be described by simple quartic force fields and which lead to strong corrections like those observed for the systems here. All other modes of the CH_3^+-He , CD_3^+-He and CH_3^+-Ne complexes were found to be converged with respect to the correlation

space and thus coupling to the critical bending mode appears to be of minor importance.

D. Tunneling splittings

As mentioned above, all vibrational calculations were based on local PESs, which include just one of the two $2p_z$ -bound minima. Attempts to generate larger PESs, which include both minima, failed due to the restriction of our program to rectilinear normal coordinates. In order to investigate the importance of tunneling, we performed several additional calculations. In a first step, we calculated the minimum energy path along the intrinsic reaction coordinate between these minima. These calculations were started at the side-bound C_{2v} transition states, which was found to be 698.5 cm^{-1} above the minima at the CCSD(T)-F12a/aug-cc-pVTZ level, but about 127 cm^{-1} below the dissociation energy (D_e). Dopfer and co-workers determined the barrier to be slightly lower at about 600 cm^{-1} .⁴ The potential energy along the intrinsic reaction coordinate (IRC) is shown in Figure 3. The IRC consists of two principal movements: (1) Starting in one minimum of the PES, the distance between the helium and the carbon atoms will substantially be increased before (2) the methyl cation starts rotating as depicted in Figure 3. Note that the C-He distance, $R(\text{C-He})$ increases from 1.817 \AA in the minimum to 3.091 \AA in the transition state. The onset for the rotation appears to be rather late and, thus, the barrier for this reaction is fairly broad. For example, at about $s = -4\text{ Bohr amu}^{1/2}$ the rotational angle $\theta(\text{HCHe})$ has changed by less than 10 degrees, but the distance has already increased by more than 0.7 \AA and the energy has increased by about 400 cm^{-1} . At the beginning of the path, the barrier is largely controlled by the C-He distance rather than the movement of the hydrogen atoms.

As the width of the potential has significant impact on the tunneling splitting, we studied this aspect in more detail and compared this IRC with that for the inversion reaction of the hydronium cation, H_3O^+ , which shows very strong tunneling splittings of up to 373 cm^{-1} for the fundamental modes.⁵⁷⁻⁵⁹ We believe that it is meaningful to compare these two systems as the barrier height of both reactions is very similar and both reactions include three tunneling hydrogen atoms. According to high-level calculations including different kinds of corrections, the barrier height for the H_3O^+ inversion was determined to be 651 or 657 cm^{-1} , respectively. For details see the work of Rajamäki *et al.*^{57,58} and Neff *et al.*⁵⁹ The comparison is shown in Figure 4. The difference is striking. The width of the barrier

for the hydronium cation is much smaller than for the $\text{CH}_3^+\text{-He}$ complex. Consequently, one would expect much smaller tunneling splittings for the rare gas complexes studied here. Moreover, as the width does not decrease very much for higher energies, one would not expect significant tunneling splittings for vibrationally excited states. This expectation is in contrast to the large tunneling splittings as predicted by the calculations of Dopfer and Luckhaus.⁴ Of course, the presented IRC is no proof that tunneling may not occur, but it is an indication that it is probably of little importance. This would be in agreement of the recent observations of Töpfer *et al.*⁹

The tunneling splitting of the vibrational ground state of the $\text{CH}_3^+\text{-He}$ complex was determined by instanton calculations. As outlined in the Computational Details, these calculations were not restricted to the local potential, which has been employed for the VCI calculations, but used the same electronic structure level, i.e. CCSD(T)-F12a/aug-cc-pVTZ, on the fly. The instanton calculations predict the tunneling splitting for the vibrational ground state to be less than 10^{-4} cm^{-1} and, thus, to be at least one to two orders of magnitude smaller than the value determined by Dopfer and Luckhaus of $8 \cdot 10^{-3} \text{ cm}^{-1}$.⁴ Our result takes into account the 3-fold degeneracy of the path in the partition function, which is caused by the three equivalent tunneling paths arising from the C_{3v} point group of the system. Note that semiclassical instanton theory has an intrinsic error bar, which is difficult to estimate. However, Richardson⁶⁰ computed the tunneling splitting of the formic acid dimer with ring-polymer instanton theory and observed an error being not larger than 20% in comparison to accurate quantum-dynamical calculations. Moreover, he concluded that it appears to be important to include all dimensions within tunneling calculations and to use an accurate PES (as we have done in our calculations) rather than using reduced dimensionality approaches.^{61,62} Therefore, we consider a value of 10^{-4} cm^{-1} to be an estimation of an upper bound, which we consider to be more reliable than the value of Dopfer and Luckhaus, which was obtained from calculations restricted to a frozen CH_3^+ moiety and to an MP2 potential of the three intermolecular coordinates only.

Again, this is no proof that significant tunneling splitting may not show up for excited vibrational states, which we could not compute directly, but it makes it rather unlikely. For that reason, we did not perform comparable calculations for the complexes with heavier rare gas atoms, in which tunneling processes are even more unlikely due to the higher mass of

the system and the pronounced covalent character of the interaction.

VI. SUMMARY AND CONCLUSIONS

High-level *ab initio* methods have been used to study the vibrational spectra of $\text{CH}_3^+\text{-Rg}$ (Rg=He, Ne, Ar, Kr) complexes. These calculations largely confirm the experimental results of Dopfer and co-workers and the conclusions of these authors that the bonding mechanism is controlled by induction for the two smaller rare gas atoms, while a covalent bond with a pronounced charge transfer can be seen for the Ar and Kr-complexes. In extension to previous studies, high-level predictions have been provided for all fundamental vibrational transitions of these complexes. These were based on variational VCI calculations relying on multidimensional potential energy surfaces obtained from explicitly correlated coupled-cluster theory. Results for the vibrational frequencies of the $\text{CH}_3^+\text{-Kr}$ complex have been provided for the first time.

The intermolecular bending modes of the $\text{CH}_3^+\text{-He}$ complex could not be determined with high accuracy due to numerical instabilities arising from the very low lying dissociation channel of the complex. The most reliable value was obtained from configuration-averaged vibrational self-consistent field theory, which was introduced to optimize the modal basis prior to the VCI calculations for degenerate states.

Reference calculations for the bare methyl cation show that corrections due to core-valence correlation, high-level coupled-cluster terms, scalar-relativistic effects and terms of higher order within the expansion of the μ -tensor are of minor importance. Consequently, standard CCSD(T)-F12b/aug-cc-pVTZ calculations already provide excellent estimates at much lower computational cost.

The aspect of tunneling splittings has been studied in detail. While tunneling splitting for vibrationally excited states could not be computed directly for technical reasons, instanton theory provides a splitting for the vibrational ground-state, which is much smaller than obtained from previous calculations. This and the very broad barrier of the potential indicates that tunneling effects might be negligible even for vibrationally excited states.

VII. ACKNOWLEDGMENTS

We are grateful to Dr. O. Asvany and B. Ziegler for valuable and insightful discussions. Moreover, we thank Prof. A. Köhn for helping us to perform CCSDT and CCSDTQ calculation using the GeCCo suite of programs. Support was provided by the COST Action CM1405 "Molecules in Motion (MOLIM)". This research was also supported in part by the bwHPC initiative and the bwHPC-C5 project provided through associated compute services of the JUSTUS HPC facility at the University of Ulm. bwHPC and bwHPC-C5 are funded by the Ministry of Science, Research and the Arts Baden-Württemberg (MWK). Further financial support was provided by the Deutsche Forschungsgemeinschaft (DFG), project RA 656/25-1.

-
- ¹ R. V. Olkhov, S. A. Nizkorodov, and O. Dopfer, *J. Chem. Phys.* **110**, 9527 (1999).
- ² O. Dopfer, R. V. Olkhov, and J. P. Maier, *J. Chem. Phys.* **112**, 2176 (2000).
- ³ R. V. Olkhov, S. A. Nizkorodov, and O. Dopfer, *J. Chem. Phys.* **108**, 10046 (1998).
- ⁴ O. Dopfer and D. Luckhaus, *J. Chem. Phys.* **116**, 1012 (2002).
- ⁵ O. Dopfer, *Int. Rev. Phys. Chem.* **22**, 437 (2003).
- ⁶ O. Asvany, S. Thorwirth, B. Redlich, and S. Schlemmer, *J. Mol. Spectrosc.* **347**, 1 (2018).
- ⁷ K. Hiraoka and I. Kudaka, *Chem. Phys. Lett.* **178**, 103 (1991).
- ⁸ D. A. Clabo Jr. and W. D. Allen and R. B. Remington and Y. Yamaguchi and H. F. Schaefer, *Chem. Phys.* **123**, 187 (1988).
- ⁹ M. Töpfer, T. Salomon, S. Schlemmer, O. Asvany, O. Dopfer, H. Kohguchi, and K. M. T. Yamada, *Phys. Rev. Lett.* **121**, 143001 (2018).
- ¹⁰ M. C. Zerner, *Int. J. Quantum Chem.* **35**, 567 (1989).
- ¹¹ W. van den Heuvel, S. Calvello, and A. Soncini, *Phys. Chem. Chem. Phys.* **18**, 15807 (2016).
- ¹² P. P. Hallmen, C. Köppl, G. Rauhut, H. Stoll, and J. van Slageren, *J. Chem. Phys.* **147**, 164101 (2017).
- ¹³ M. Neff, T. Hrenar, D. Oschetzki, and G. Rauhut, *J. Chem. Phys.* **134**, 064105 (2011).
- ¹⁴ J. K. G. Watson, *Mol. Phys.* **15**, 479 (1968).

- ¹⁵ J. M. Bowman and T. Carrington Jr. and H. D. Meyer, *Mol. Phys.* **106**, 2145 (2008).
- ¹⁶ B. Ziegler and G. Rauhut, *J. Chem. Phys.* **144**, 114114 (2016).
- ¹⁷ J. M. Bowman, *Acc. Chem. Res.* **19**, 202 (1986).
- ¹⁸ J. M. Bowman, *J. Chem. Phys.* **68**, 608 (1978).
- ¹⁹ R. Gerber and M. Ratner, *Adv. Chem. Phys.* **70**, 97 (1988).
- ²⁰ W. H. Miller, *J. Chem. Phys.* **62**, 1899 (1975).
- ²¹ A. I. Vainshtein, V. I. Zakharov, V. A. Novikov, and M. A. Shifman, *Sov. Phys. Usp.* **25**, 195 (1982).
- ²² G. Mil'nikov and H. Nakamura, *Phys. Chem. Chem. Phys.* **10**, 1374 (2008).
- ²³ J. O. Richardson and S. C. Althorpe, *J. Chem. Phys.* **134**, 054109 (2011).
- ²⁴ J. O. Richardson, S. C. Althorpe, and D. J. Wales, *J. Chem. Phys.* **135**, 124109 (2011).
- ²⁵ T. B. Adler, G. Knizia, and H.-J. Werner, *J. Chem. Phys.* **127**, 221106 (2007).
- ²⁶ D. E. Woon and T. H. D. Jr, *J. Chem. Phys.* **98**, 1358 (1993).
- ²⁷ G. Rauhut, G. Knizia, and H. Werner, *J. Chem. Phys.* **130**, 054105 (2009).
- ²⁸ H.-J. Werner, P. J. Knowles, R. Lindh, F. R. Manby, M. Schütz, et al., *Molpro, development version 2018.2, a package of ab initio programs* (2018), see <http://www.molpro.net>.
- ²⁹ M. Neff and G. Rauhut, *J. Chem. Phys.* **131**, 124129 (2009).
- ³⁰ M. Neff and G. Rauhut, *J. Chem. Phys.* **131**, 229901 (2009).
- ³¹ B. Ziegler and G. Rauhut, *J. Chem. Phys.* **149**, 164110 (2018).
- ³² J. B. Rommel, T. P. M. Goumans, and J. Kästner, *J. Chem. Theory Comput.* **7**, 690 (2011).
- ³³ J. Kästner, J. M. Carr, T. W. Keal, W. Thiel, A. Wander, and P. Sherwood, *J. Phys. Chem. A* **113**, 11856 (2009).
- ³⁴ S. Metz, J. Kästner, A. A. Sokol, T. W. Keal, and P. Sherwood, *WIREs Comput. Mol. Sci.* **4**, 101 (2014).
- ³⁵ H. P. Hratchian and H. B. Schlegel, *J. Chem. Phys.* **120**, 9918 (2004).
- ³⁶ H. P. Hratchian and H. B. Schlegel, *J. Chem. Theory Comput.* **1**, 61 (2005).
- ³⁷ J. Meisner, M. N. Markmeyer, M. U. Böhner, and J. Kästner, *Phys. Chem. Chem. Phys.* **19**, 23085 (2017).
- ³⁸ A. E. Reed, R. B. Weinstock, and F. Weinhold, *J. Chem. Phys.* **83**, 735 (1985).
- ³⁹ A. Hesselmann, G. Jansen, and M. Schütz, *J. Chem. Phys.* **122**, 014103 (2005).
- ⁴⁰ M. W. Crofton, M.-F. Jagod, B. D. Reh fuss, W. A. Kreiner, and T. Oka, *J. Chem. Phys.* **88**,

666 (1988).

- ⁴¹ T. Koenig, T. Balle, and W. Snell, *J. Am. Chem. Soc.* **97**, 662 (1975).
- ⁴² T. Koenig, T. Balle, and J. C. Chang, *Spectrosc. Lett.* **9**, 755 (1976).
- ⁴³ J. Dyke, N. Jonathan, E. Lee, and A. Morris, *J. Chem. Soc., Faraday Trans. II* **72**, 1385 (1976).
- ⁴⁴ X. Liu, R. L. Gross, and A. G. Suits, *Science* **294**, 2527 (2001).
- ⁴⁵ B. K. Cunha de Miranda, C. Acaraz, M. Elhanine, B. Noller, P. Hemberger, I. Fischer, G. A. Garcia, H. Soldi-Lose, B. Gans, L. A. Viera Mendes, et al., *J. Phys. Chem. A* **114**, 4818 (2010).
- ⁴⁶ H.-G. Yu and T. Sears, *J. Chem. Phys.* **117**, 666 (2002).
- ⁴⁷ M. Keceli, T. Shiozaki, K. Yagi, and S. Hirata, *Mol. Phys.* **107**, 1283 (2009).
- ⁴⁸ M. Ragni, A. C. P. Bitencourt, F. V. Prudente, P. R. P. Barreto, and T. Posati, *Eur. Phys. J. D* **70**, 60 (2016).
- ⁴⁹ M. Reiher and A. Wolf, *J. Chem. Phys.* **121**, 2037 (2004).
- ⁵⁰ M. Reiher and A. Wolf, *J. Chem. Phys.* **121**, 10945 (2004).
- ⁵¹ M. Hanauer and A. Köhn, *J. Chem. Phys.* **131**, 124118 (2009).
- ⁵² M. Hanauer and A. Köhn, *J. Chem. Phys.* **134**, 204111 (2011).
- ⁵³ T. A. Ruden, T. Helgajær, P. Jørgensen, and J. Olsen, *J. Chem. Phys.* **121**, 5874 (2004).
- ⁵⁴ J. Koput and K. A. Peterson, *J. Chem. Phys.* **125**, 044306 (2006).
- ⁵⁵ P. Meier, M. Neff, and G. Rauhut, *J. Chem. Theory Comput.* **7**, 148 (2011).
- ⁵⁶ G. Rauhut, V. Barone, and P. Schwerdtfeger, *J. Chem. Phys.* **125**, 054308 (2006).
- ⁵⁷ T. Rajamäki, M. Kallay, J. Noga, P. Valiron, and L. Halonen, *Mol. Phys.* **102**, 2297 (2004).
- ⁵⁸ T. Rajamäki, A. Miani, and L. Halonen, *J. Chem. Phys.* **118**, 10929 (2003).
- ⁵⁹ M. Neff and G. Rauhut, *Spectrochim. Acta A* **119**, 100 (2014).
- ⁶⁰ J. O. Richardson, *Phys. Chem. Chem. Phys.* **19**, 966 (2017).
- ⁶¹ A. N. Beyer, J. O. Richardson, P. J. Knowles, J. Rommel, and S. C. Althorpe, *JCP* **7**, 4374 (2016).
- ⁶² J. O. Richardson, *J. Chem. Phys.* **148**, 200901 (2018).

Figures

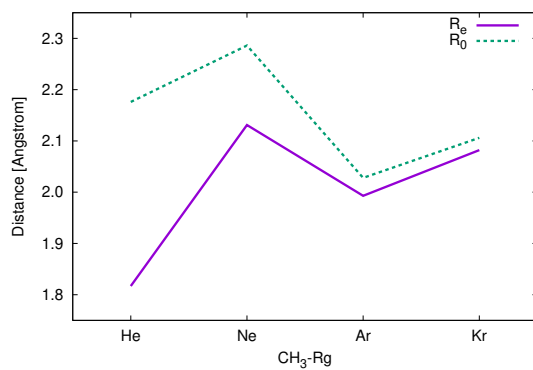


Figure 1: Equilibrium (purple, solid) and vibrationally averaged (green, dotted) distances of the rare gas atoms to the carbon atom in CH_3^+-Rg complexes ($\text{Rg}=\text{He}, \text{Ne}, \text{Ar}, \text{Kr}$).

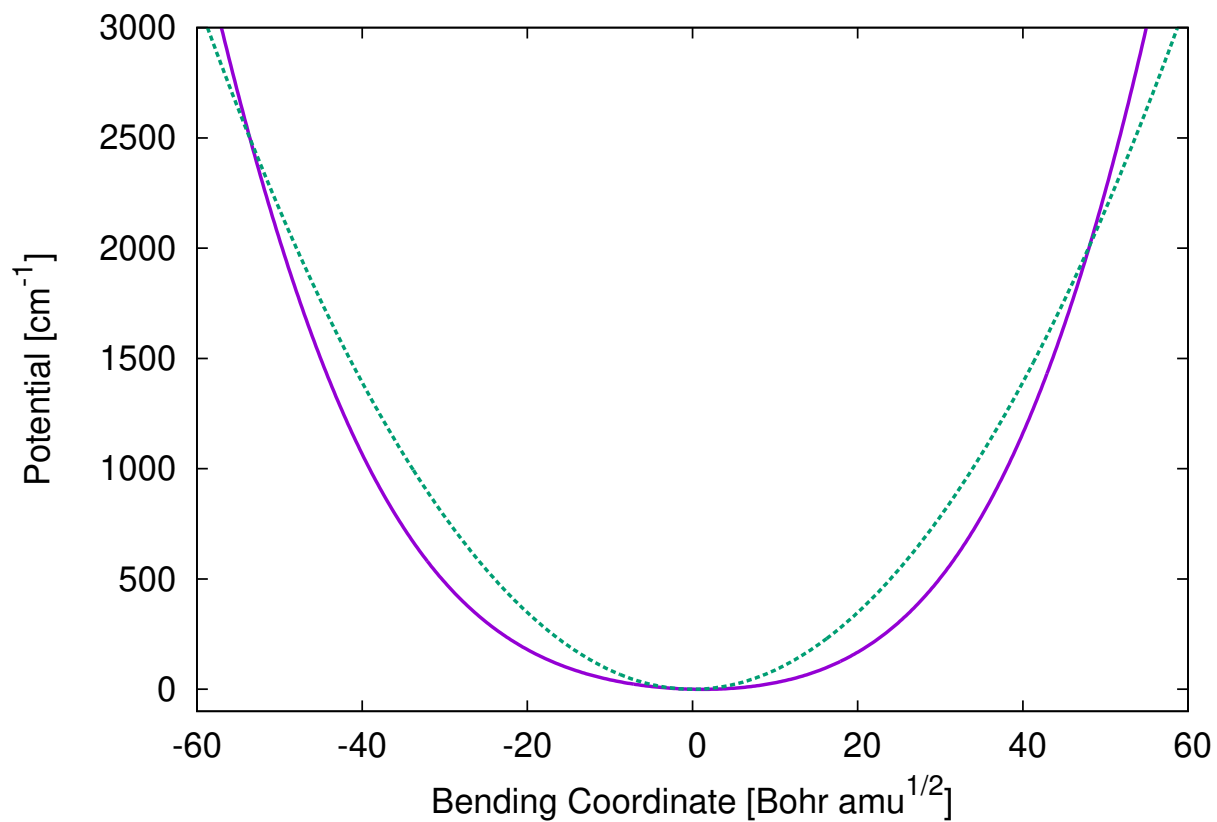


Figure 2: Comparison of the harmonic potential (green, dotted) in comparison to the effective anharmonic VSCF potential (purple, solid) along the intermolecular bending mode of CH_3^+-He .

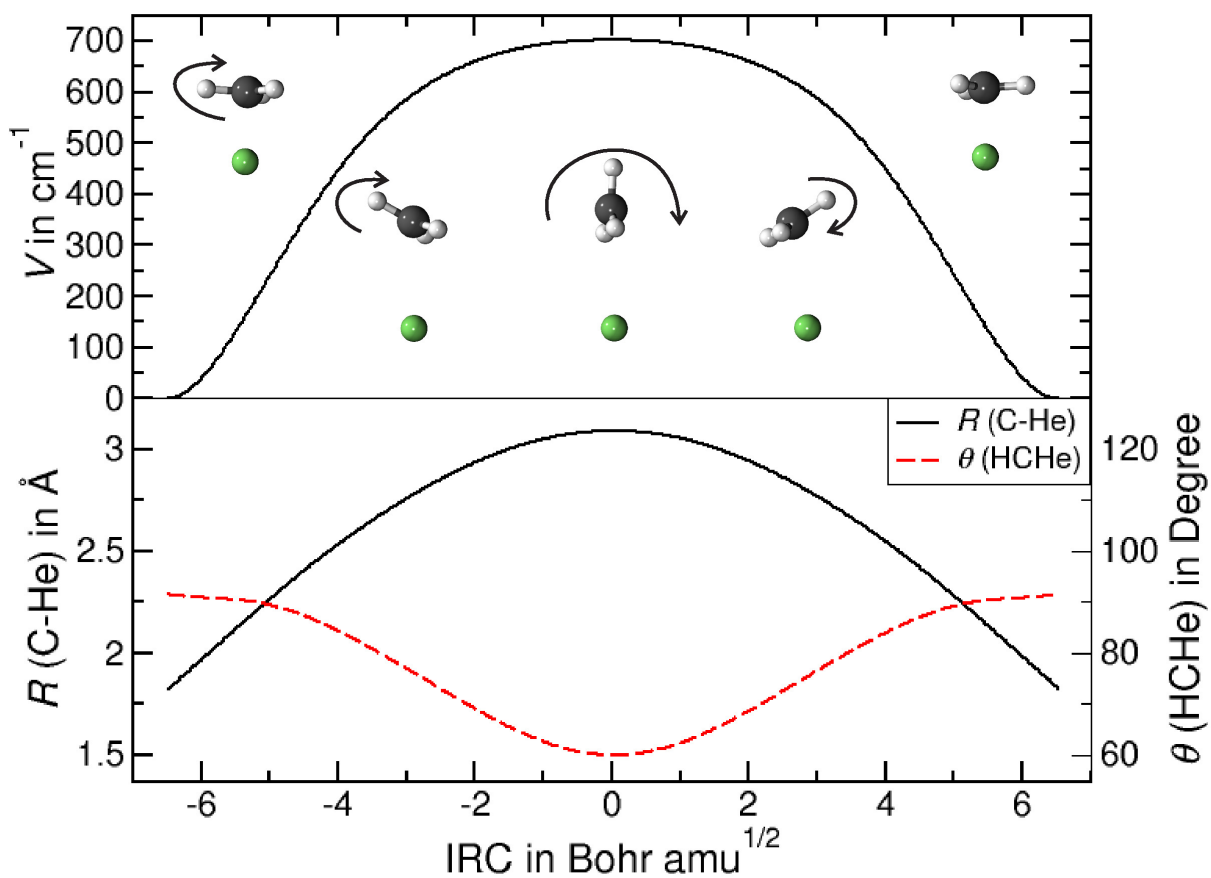


Figure 3: Top: Potential energy along the minimum energy path for the intrinsic rotation of the methyl cation within the $\text{CH}_3^+\text{-He}$ complex. Bottom: Variation of the C-He distance $R(\text{C-He})$ (black solid) and the angle $\theta(\text{HCHe})$ (red dashed) along the same pathway.

Figure 4: Comparison of the IRCs based on CCSD(T)-F12a calculations of inversions of $\text{CH}_3^+ - \text{He}$ (black) and the H_3O^+ (red dashed). Note, however, that the coordinates of the respective systems are obviously not the same.

Tables

Table I: Structural parameters of $\text{CH}_3^+ - \text{Rg}$ ($\text{Rg} = \text{He, Ne, Ar, Kr}$) complexes. Values are given in Ångström or degree.

Complex	$\theta_e(\text{HCRg})^a$	$R_e(\text{C-Rg})^a$	$R_0(\text{C-Rg})^a$	$\Delta R_{e0}(\text{C-Rg})^{a,b}$	$\Delta R_e(\text{C-H}_3)^c$
$\text{CH}_3^+ - \text{He}$	91.51 (91.4)	1.817 (1.834)	2.178 (2.176)	0.361 (0.34)	0.029
$\text{CH}_3^+ - \text{Ne}$	91.31 (91.4)	2.131 (2.135)	2.286 (2.300)	0.155 (0.17)	0.025
$\text{CH}_3^+ - \text{Ar}$	98.83 (99.0)	1.993 (1.988)	2.030 (2.053)	0.038 (0.10)	0.166
$\text{CH}_3^+ - \text{Kr}$	100.51	2.082	2.106	0.025	0.198

^a Values in parentheses were taken from Ref. 5 and refer to MP2/aug-cc-pVTZ calculations. Note that our $R_0(\text{C-Rg})$ and $\Delta R_{e0}(\text{C-Rg})$ values rely on a different definition than Dopfer's R_{cm} and $R_{cm} - R_e$ values given in parentheses.

^b Difference of the C-Rg bond length between the equilibrium and the vibrationally averaged structure.

^c Out-of-plane distortion of the carbon atom relative to the plane defined by the three hydrogen atoms within the equilibrium structure.

Table II: Structural parameters of $\text{CD}_3^+ - \text{Rg}$ ($\text{Rg} = \text{He, Ne, Ar, Kr}$) complexes. Values are given in Ångström.

Complex	$R_0(\text{C-Rg})$	$\Delta R_{\text{e0}}(\text{C-Rg})^a$
$\text{CD}_3^+ - \text{He}$	2.102	0.285
$\text{CD}_3^+ - \text{Ne}$	2.257	0.122
$\text{CD}_3^+ - \text{Ar}$	2.023	0.030
$\text{CD}_3^+ - \text{Kr}$	2.102	0.020

^a Difference of the C-Rg bond length between the equilibrium and the vibrationally averaged structure.

Table III: Interaction energies of $\text{CH}_3^+ - \text{Rg}$ (Rg=He, Ne, Ar, Kr). Values are given in cm^{-1} .

Complex	E_{Cplx}^a	E_{Relax}^a	D_{e}^a	D_0
$\text{CH}_3^+ - \text{He}$	886.7 (761.6)	61.1 (54.5)	825.6 (707.1)	247.1
$\text{CH}_3^+ - \text{Ne}$	1241.5 (1011.2)	46.8 (57.7)	1194.7 (958.5)	663.7
$\text{CH}_3^+ - \text{Ar}$	8650.7 (7781.6)	2073.0 (2206.0)	6577.7 (5575.6)	5428.4
$\text{CH}_3^+ - \text{Kr}$	12579.6	2929.9	9649.7	8486.2

^a Values in parentheses were taken from Ref. 5 and refer to MP2/aug-cc-pVTZ calculations.

Table IV: Harmonic and anharmonic vibrational frequencies of CH_3^+ and CD_3^+ . Values are given in cm^{-1} .

		CH_3^+				CD_3^+		
Mode	Sym.	Harm.	VCI ^a	VCI ^b	Exp. ^c	Harm.	VCI ^a	Exp. ^d
ZPVE	a'_1	6908.6	6807.5	6816.6		5101.3	5046.0	
ν_1	a'_1	3043.4	2940.2	2943.7		2153.1	2095.7	
ν_2	a''_2	1424.5	1405.0	1406.7		1103.6	1091.3	1090
ν_3	e'	3244.0	3104.9	3109.8	3108.4	2422.2	2343.1	2337
ν_4	e'	1430.7	1393.6	1395.9		1050.7	1030.0	1027

^a Obtained from CCSD(T)-F12b/cc-pVTZ-f12 calculations.

^b Obtained from CCSD(T)-F12b/cc-pVQZ-f12 calculations and additional corrections for core-valence electron correlation, scalar-relativistic effects and high-order coupled-cluster terms (see text).

^c Experimental data taken from Ref. 40

^d Experimental data taken from Ref. 6

Table V: Harmonic and anharmonic vibrational frequencies of $\text{CH}_3^+ - \text{Rg}$ (Rg=He, Ne, Ar, Kr).

Value are given in cm^{-1} .

Mode	Sym.	CH ₃ ⁺ -He			CH ₃ ⁺ -Ne			CH ₃ ⁺ -Ar			CH ₃ ⁺ -Kr			
		Harm.	3D ^a	VPT2 ^b	VCI	Exp. ^c	Harm.	VCI	Exp. ^d	Harm.	VCI	Exp. ^e	Harm.	VCI
ZPVE	<i>a</i> ₁	7649.4			7386.0		7508.9	7338.5		8081.6	7956.8		8088.7	7971.0
<i>ν</i> ₁	<i>a</i> ₁	3058.6		2935	2944.5	2946.4	3060.1	2949.9		3091.0	2975.4	2979 ^f	3093.2	2979.6
<i>ν</i> ₂	<i>a</i> ₁	1408.2		1391	1383.8	1402	1406.8	1380.4		1360.2	1329.4		1336.9	1304.6
<i>ν</i> _s	<i>a</i> ₁	216.6	83	122	138.3		182.0	147.0		374.4	338.7		402.1	377.2
<i>ν</i> ₃	<i>e</i>	3260.9		3104	3113.5	3115.0	3262.1	3119.3	3119.4	3271.0	3129.9	3145(30)	3264.1	3123.2
<i>ν</i> ₄	<i>e</i>	1429.3		1395	1393.4	1383	1431.4	1393.5		1437.9	1397.0		1442.5	1402.9
<i>ν</i> _b	<i>e</i>	617.5	128/149	237	(322) ^g		491.0	(375) ^g		959.9	917.0		966.1	939.4

^a Variational 3D frequencies obtained from MP2/aug-cc-pVTZ calculations. Taken from Ref. 4.

^b Anharmonic VPT2 frequencies based on CCSD(T)/aug-cc-pVTZ calculations, taken from Ref. 6.

^c Experimental data taken from Refs. 6,9.

^d Experimental data taken from Ref. 2.

^e Experimental data taken from Ref. 3.

^f Estimated from a local mode-coupled Morse oscillator model.

^g Numerically not stable, see text.

Table VI: Harmonic and anharmonic vibrational frequencies of $\text{CD}_3^+ \text{-Rg}$ (Rg=He, Ne, Ar, Kr). Value are given in cm^{-1} .

		$\text{CD}_3^+ \text{-He}$		$\text{CD}_3^+ \text{-Ne}$		$\text{CD}_3^+ \text{-Ar}$		$\text{CD}_3^+ \text{-Kr}$	
Mode	Sym.	Harm.	VCI	Harm.	VCI	Harm.	VCI	Harm.	VCI
ZPVE	a_1	5677.6	5522.8	5552.4	5455.5	5975.8	5906.4	5979.1	5914.3
ν_1	a_1	2164.4	2092.4	2164.9	2092.2	2192.9	2144.9	2196.8	2147.2
ν_2	a_1	1078.2	1073.3	1079.8	1031.8	1011.3	995.5	993.6	975.7
ν_s	a_1	213.8	142.0	174.8	141.1	364.8	336.9	386.9	367.9
ν_3	e	2435.7	2350.6	2436.4	2353.9	2440.1	2359.1	2433.1	2353.4
ν_4	e	1050.1	1030.3	1052.5	1031.8	1052.5	1032.7	1053.6	1026.6
ν_b	e	463.6	(262) ^a	354.3	280.9	698.7	637.4	703.6	687.9

^a Numerically not stable, see text.

Table VII: Comparison of the intermolecular coupling modes ν_b and ν_s obtained from ground-state based VCI calculations (gs-VCI) and state-specific VCI calculations (ss-VCI).

Complex	ν_b		ν_s	
	gs-VCI	ss-VCI ^a	gs-VCI	ss-VCI ^b
CH ₃ ⁺ -He	336.5	322.0	138.3	138.1
CD ₃ ⁺ -He	269.8	261.5	142.0	141.8
CH ₃ ⁺ -Ne	379.5	374.6	147.0	147.0
CD ₃ ⁺ -Ne	283.3	280.9	141.2	141.1

^a Using modals from CAVSCF theory.

^b Using modals from state-specific VSCF calculations.